# ELECTROKINETIC-POTENTIAL FLUCTUATIONS PRODUCED BY PIPE-FLOW TURBULENCE

by

Dr. Hsing Chuang, Research Engineer

and

Dr. J. E. Cermak, Professor of Civil Engineering and Engineering Mechanics

Civil Engineering Department
Colorado State University
Fort Collins, Colorado



Paper to be Submitted to
The ~~Physics of Fluids~~
A. I. Ch. E.

July 1964

CER62HC-JEC47

LIST OF FIGURES


| Figure No. | Figure Title |
|---|---|
| 1 | Test Section |
| 2 | Flow System and Electrical Measurement Equipment |
| 3 | Probes |
| 4 | Probes |
| 5 | Electrical Measurement Equipment for Turbulent Shearing Stress Measurement |
| 6 | Turbulent Shearing Stress Distribution |
| 7 | Turbulent Intensity of u' across the Pipe |
| 8 | Turbulent Intensity of v' across the Pipe |
| 9 | Turbulent Intensity of w' across the Pipe |
| 10 | Double-Correlation-Coefficient Distribution |
| 11 | Distribution of v'/u' across the Pipe |
| 12 | Distribution of w'/u' across the Pipe |
| 13 | Spectra of $E_u$ , Re = 51,000 |
| 14 | Spectra of $E_v$ , Re = 51,000 |
| 15 | Spectra of $E_w$ , Re = 51,000 |
| 16 | Spectra of $E_{uv}$ , Re = 51,000 |

## ABSTRACT

The distribution across a pipe of turbulent intensities, shearing stress, and energy spectra are inferred from measured electrokinetic-potential fluctuations in a fully developed flow of distilled water in a 2.54 cm diameter glass pipe. These quantities are shown to be in good agreement with those obtained by Laufer and Sandborn with hot-wire anemometers for air flows at the same mean Reynolds number.

A tentative analytical model of the phenomena is constructed and analyzed by Maxwell's electrodynamic field equations for a nonmagnetized medium moving with a velocity which is much smaller than the velocity of light. A set of equations governing the interrelation between the electro-kinetic-potential fluctuations and the turbulent velocity-fluctuation components of the flow field in fully developed pipe flow is deduced. The equations are simplified and assumed to have the form: $\sigma \nabla \psi = \overline{\rho \underline{u}}$ . Fourier transforms are then introduced and simple relations between the electrokinetic-potential fluctuations and velocity fluctuations are obtained.

# INTRODUCTION

The electrokinetic phenomenon was first observed early in the 19th century. The basic idea of an electrical double layer or diffused double layer arising from adsorption of fluids in contact with solid walls was formed and developed during the last hundred years. The fundamental formulation of the electrokinetic phenomenon is attributed to Helmholtz. However, all early experiments and theories of the electrical double layer were concerned with either a laminar flow through a small tube or a flow through a porous diaphragm connecting two liquid containers. Only recently has the study of electrokinetics been extended to turbulent shear flow.

The instantaneous fluctuations of the streaming potential which occur in a turbulent flow were first observed and recorded by Bocquet [1]. Binder [2] was the first researcher to use electrokinetic measurements to infer velocity fluctuations near the wall in a turbulent fluid. Chuang [3] has used it to infer velocity fluctuations in a fully developed pipe flow.

Because of the many experimental difficulties which arise, it is impossible to explore the characteristics of turbulent motion very close to a wall with existing techniques. Our present knowledge of turbulent shear flow in close proximity to a wall is still insufficient to be the basis for a sound and complete theory. It was this particular problem which motivated this study of electrokinetics in a turbulent flow of distilled water.

---


[1] Bocquet, P. E., Sliepcevich, C. M., and Bohr, D. F.: Effect of Turbulence on the Streaming Potential. Indust. Engr. Chem., 48, 197-200, 1956.

[2] Binder, G. J.: Electrokinetic-Potential Fluctuations Produced by Turbulence at a Solid-Liquid Interface. Doctoral Dissertation, Colorado State University, Fort Collins, Colorado, 1960, 121p.

[3] Chuang, H.: Electrokinetic-Potential Fluctuations Produced by Turbulence in Fully Developed Pipe Flow. Doctoral Dissertation, Colorado State University, Fort Collins, Colorado, 1962, 111p.

## EXPERIMENTAL EQUIPMENT AND PROCEDURE

The experimental equipment consists of the flow system, the electrodes, and the electrical measurement equipment.

The flow system is a self-circulating facility as shown in figure 2. It has a constant-head tank, 6 in. in diameter, which provides a constant head of 11 ft., upstream and downstream reservoirs, a stainless steel pump driven by a 1/2-hp. electric motor and a long length of circular glass pipe. These components are interconnected by Tygon tubing and are made of relatively inert materials. The circular pipe consists of nine pieces of glass and "Lucite" pipes of various lengths, all 2.54 cm in inside diameter. The pipe sections are connected together by precision couplings. The test section which is shown in figure 1 can thus be inserted at various axial positions. The total length of the pipe available is about 5.1 m. The flow rate in the pipe is regulated by the valves located at the downstream end of the pipe and is stabilized by regulating the outflow from each reservoir. Equilibrium water with a conductivity of about $5 \times 10^{-4}$ mhos per meter at $20^{\circ}C$ was used as the fluid throughout this work.

The electrodes are made of magneto wire (i.e., varnished, commercial grade copper) of 0.16 and 0.20 mm in diameter. The electrodes are supported by a probe of stainless steel tubing. As shown in figures 3 and 4, three kinds of probes have been used. The cylindrical probe is made by drilling a hole on the tube wall, inserting two insulated magneto wires into the tube through the hole, and then gluing them to the tube with an epoxy cement. The electrodes are fastened closely and aligned in such a manner that when the probe moves up and down in the radial direction, the electrodes are in the circumferential direction. The same method of construction was used in making the T-shaped probes but different sizes of the magneto wire and external tubing were used. This type of electrode alignment is used to measure the circumferential electrokinetic-potential fluctuations due to the velocity fluctuation in this direction. The probe for the measurement of electrokinetic-potential fluctuations due to the turbulent shearing stress and the turbulent velocity fluctuations in both the axial and the radial

directions have four electrodes, two electrodes for each direction which are fastened closely and aligned in each direction. The probe is inserted into the pipe through the slot in the test section and is connected to a micrometer which is supported by a rigid frame. Experimental evidence reveals no quantitative difference in the measured signals due to the difference in wire size (0.16 and 0.20 mm) or the difference in external tube size (0.80 and 1.25 mm).

The electrical measurement equipment is shown in figures 2 and 5. The equipment shown in figure 2 is for the measurement of the distribution and the spectral density function of the turbulent intensities across the pipe while that shown in figure 5 is for the measurement of the spatial distribution and spectral density distribution of the shearing stress across the pipe. The low-level differential pre-amplifier (Tektronix Type 122) was used to amplify the signal. This amplifier has selective gain and frequency response ranges which were set at 1000x and from 0.2 to 10,000 cps respectively throughout the measurements. The output of the pre-amplifier was then fed into either a wave analyzer (Hewlett-Packard Model 300A), or an RMS meter (Hewlett-Packard Model 400H), or an oscilloscope (Tektronix Type 502). The wave analyzer with a frequency response range from 20 to 16,000 cps has a narrow band pass of less than 10 cps at the half-power point. However, at frequencies near zero, the wave analyzer's selectivity is not well defined so that the spectral data were taken only at frequencies above 30 cps. The RMS meter has a voltage range from 0.1 millivolt to 300 volts and a frequency response range from 10 to $4 \times 10^6$ cps. The oscilloscope is used for viewing the randomness of the potential fluctuations and of detecting any anomaly such as "spikes" or 60-cycle pickup. The impedance between the electrodes through the liquid, in parallel with the input impedance of the pre-amplifier of about $10^7$ ohms, is computed to be about $10^5$ ohms. The time constant is estimated to be about $5 \times 10^{-6}$ second which is smaller than the period of the highest frequency to be passed by the pre-amplifier, i.e., $10^{-4}$ second, so that the amplifying circuit is adequate. A true root-mean-square analyzer (Hubbard Instrument Model L)

with adding and subtracting channels was used for the instantaneous signal addition and subtraction. The external probe tubing and some other points of the system were grounded as shown in figure 2. After the completion of the research reported here, it has been found that AC power sources inside the shielded cage do not affect the electrode signals. However all the data reported herein were taken without AC power within the cage. The overall noise was measured before each run and the corresponding readings were corrected for the noise [3] .

The usual experimental procedure consisted of an electronic instruments warm-up period and a calibration before and during the data acquisition. Therefore, there should be little systematic error in the data due to instrument drift. The flow rate which could be changed by regulating the downstream valve was determined at the beginning of each run. Some electrode measurements were made at two sections of the pipe 290 cm and 411 cm from the pipe entrance. These data exhibited no systematic difference, which implies that the flow was fully developed. Subsequently, measurements were made only at the downstream section.

## DISCUSSION OF EXPERIMENTAL RESULTS

### Turbulent Shearing Stress Distribution -

The turbulent shearing stress was deduced from the measured electrokinetic-potential-difference fluctuation using equation 6 at $y/a = 0.15$, 0.20, 0.25, 0.35, 0.45, 0.55, 0.65, 0.75, 0.85, 0.95, and 1.00 (center of the pipe) for Reynolds numbers 66,000, 51,000, 46,000, 31,000 and 17,000. The results are shown in figure 6 where $K$ is an arbitrary constant and is equal to about $10^{-10}$ in this case. The solid line represents Pai's equation [4] with the arbitrary constants $n$ and $s$ determined from Laufer's experimental data [5] at Reynolds number $5 \times 10^4$. The results for Reynolds numbers, 31,000 and 17,000 were discarded because of the lower signal-to-noise ratio of the electrokinetic measurements at these runs.

### Turbulent Intensity Correlations -

As discussed in the theory section, at any wave number $n$, the spectral distributions of $E_u$, $E_v$, and $E_w$, are assumed to be directly proportional to the respective spectral distributions of $E_{\Delta\psi x}$, $E_{\Delta\psi r}$, and $E_{\Delta\psi\theta}$. When these quantities are integrated over all contributing frequencies, they will give the mean-square values for overall frequency range. The turbulent intensities inferred from the electrokinetic-potential data which were taken at those points mentioned in the previous paragraph for the same Reynolds numbers were computed. Since the probes were not calibrated, only the functional forms of the turbulent intensity distributions across the pipe radius could be obtained. (The calibration technique for the electrokinetic-potential fluctuation sensitive probes

---

[4] Pai, S. I.: On Turbulent Flow in Circular Pipe. J. Franklin Inst., 256: 337-352, 1953.

[5] Laufer, J.: The Structure of Turbulence in Fully Developed Pipe Flow. NACA TN 2954, 1953, 53 p.

has not been studied in this work in a direct manner.) The results are shown in figures 7, 8, and 9 where isotropy has been assumed at the center of the pipe thereby forcing equality at this point at the highest Reynolds number. All inferred turbulent intensities decrease rapidly with Reynolds number. Again the results for Reynolds numbers 31,000 and 17,000 were discarded for the reason mentioned before. For the purpose of comparison, the functional forms of Laufer's experimental data are also plotted in these figures; all electrokinetic data show good agreement with Laufer's results for the same Reynolds number. When the distributions of the inferred turbulent intensities across the pipe for each Reynolds number are compared with one another, it shows the degree of anisotropy increasing toward the wall in every case.

The double-correlation-coefficient was computed from the inferred turbulent shearing stress and intensity data. The result is shown in figure 10. Again good agreement with Laufer's anemometer data is revealed for the same Reynolds number. The double-correlation-coefficient deduced from Sandborn's experimental data [6] is also plotted in the figure and they show even better agreement with the present results.

The relative values of turbulent intensities are plotted in figures 11 and 12. As mentioned before, a local isotropy at the center of the pipe is assumed to force $v'/u'$ to unity at this point for the highest Reynolds number. This assumption is not necessarily true for low Reynolds numbers such as those considered in this experiment. Since $w'$ should be equal to $v'$ at the center of the pipe, the same values of $u'$ shown in $v'/u'$ was used to compute $w'/u'$. The degree of anisotropy is thus shown more clearly to increase toward the pipe wall. These data also indicate the degree of anisotropy of the turbulent intensities of the radial and the circumferential components which were inferred from the measured electrokinetic-potential-difference fluctuation. All data for Reynolds numbers around $5 \times 10^4$ show good agreement with Laufer's experimental data obtained by using hot-wire

---

[6] Sandborn, V. A.: Experimental Evaluation of Momentum Terms in Turbulent Pipe Flow. NACA TN 3266, 1955, 40 p.

anemometers in air flows. The relative values of turbulent intensities calculated from Sandborn's experimental data are also shown. The anisotropy at the center of the pipe is more pronounced for these data.

Spectra of $E_u$ , $E_v$ , $E_w$ , and $E_{uv}$ -

The spectral distributions of the electrokinetic-potential fluctuations in every direction show continuous increase with Reynolds number which is consistent with the assumed interrelation between the electrokinetic-potential fluctuations and the turbulent velocity fluctuations, because the intensity of turbulence $u_i'$ of the flow field increases with Reynolds number as shown experimentally by Sandborn [6] . The relation shown in equation 6 is therefore supported by the experimental data obtained to date. For the present probes and amplifier settings, equation 6 may be written as follows [3] :

$$E_{u\,,\,v\,,\,w\,,\,uv}(n) = 1.25 \times 10^{-2}\, E_{\Delta\Psi x\,,\,r\,,\,\theta\,,\,xr}(n) \quad .$$

The spectral distribution of turbulent energy and shearing stress were computed as shown in figures 13 to 16, which are now examined in order to gain some further insight into the turbulent shear flow. Theoretical analysis of the energy spectrum in nonisotropic homogeneous turbulence with a uniform mean flow is summarized by Hinze [7] . Because of the complexity of the problem near a solid boundary when mean turbulent shearing stresses are present, no theory on the turbulent energy spectrum in nonisotropic wall turbulence has yet been developed. Nevertheless, electrokinetic measurements of the spectral distributions of turbulent energy and shearing stress in this type of flow may be of assistance in studying the turbulent shear flow.

The mechanism of turbulent shear flow consists of production, diffusion, transfer, convection, and dissipation of turbulent energy. In general, the

---

[7] Hinze, J. O.: Turbulence. McGraw-Hill, New York 1959, 586 p.

effects of the diffusion and convection of turbulent energy are assumed to be confined to the very low wave numbers which lie outside the equilibrium range and are negligible in the wave number range measured in this experiment. By assuming that the production of turbulent energy predominates in the low-wave number region or large eddies, Tchen [8] predicted a spectral distribution varying as $n^{-1}$ for this region. This low wave number region is generally observed only in the spectra of the turbulent velocity component in the direction of the main flow in low-speed air flows. The transfer region is characterized by a spectral variation of $n^{-5/3}$ and this region exists over a wide wave number range where the turbulent energy is transferred from the larger eddies to the smaller eddies through the spectrum without being significantly influenced by the turbulent energy production or dissipation mechanisms. This concept is limited to large turbulent Reynolds numbers and it has received some experimental support from Laufer [5] . For the higher wave number range, the viscous dissipation mechanism predominates and the spectral variation is $n^{-7}$ . However, experimental data by many researchers indicate a continuously increasing slope exceeding the negative power of 7.

The inferred $E_u$ spectra, as shown in figure 13, have only limited ranges of the -1 and -5/3 powers of the wave number $n$ , however, these curves vary as a -7/2 power of $n$ over a considerable range. This phenomenon might indicate some characteristic inherited to the nonisotropic wall turbulent flow in low Reynolds numbers. Experimental data taken by Sandborn at the pipe center for Reynolds number $5 \times 10^4$ are also plotted in the figure and a good agreement is revealed (once again, a single data point at one frequency was forced to fit Sandborn's data in order to eliminate the undetermined calibration constant from equation 6). The -1 power of $n$ is absent in $E_v$ and $E_w$ spectra as seen in figures 14 and 15. The -5/3 and -7/2 powers of $n$ are indicated to take place over considerable ranges for Reynolds number 51,000, however, in lower Reynolds number, only the -5/2 power of $n$ occurs over an appreciable range. These

---

[8] Tchen, C. M.: On the Spectrum of Energy in Turbulent Shear Flow. U.S. Nat. Bur. Standards, Res. Paper RP 2388, J. Res., 50:51-62, 1953.

phenomena might also disclose a characteristic of the flow in low Reynolds number. The spectra of $E_v$ and $E_w$ are significantly different from those of $E_u$ in the smaller wave number region and the absence of -1 power of $n$ in these spectra has thus confirmed the prediction by Tchen [8] .

The spectral distribution of turbulent shearing stress is shown in figure 16. These spectra are valuable for a direct test of local isotropy as discussed by Klebanoff [9] . The present experimental data when compared with his data, indicate that no local isotropy has been attained.

---

[9] Klebanoff, P. S.: Characteristics of Turbulence in a Boundary Layer with Zero Pressure Gradient. NACA Rep. 1247, 1955, 19 p.

## TENTATIVE THEORY

Fully developed turbulent motion of an incompressible fluid flowing in a pipe of circular cross-section will be studied. It has the property of homogeneity in both the longitudinal and the circumferential directions; thus all Eulerian time-mean values at a given point are functions of $r$ , the radial coordinate only.

In turbulent motion both scalar and vector quantities exhibit random fluctuations, and generally, some correlations should exist among them. As discussed by Binder [2] , electrokinetic-potential fluctuations are generated whenever the true charge-density is transported in the turbulent flow field. It is therefore a general objective of this analysis to find some correlation between the electrokinetic-potential fluctuations and the velocity-fluctuation components.

Maxwell's electrodynamic field equations [10] for a nonmagnetized medium moving with a velocity $\underline{U}$ which is small compared to the velocity of light, together with the generalized Ohm's law and the equation of mass conservation for an incompressible fluid, yield the equation of continuity for electrodynamics in a moving medium. After some mathematical manipulation and simplification, this relation may be written as [3] :

$$\frac{\partial \rho}{\partial t} + (\underline{U} \cdot \nabla)\ \rho + \frac{\rho}{\tau} = 0 \qquad (1)$$

where $\rho$ is the true charge-density and $\tau$ is the relaxation time of the medium. The relaxation time is a characteristic time of the fluid and represents the time necessary for restoration of the original equilibrium charge distribution after the initiation of a disturbance.

Equation 1 shows that the sum of the material derivative of true charge-density and the change of true charge-density during the time $\tau$ is equal to zero. By separating the turbulent quantities in equation 1 into a

---

[10] Panofsky, W. K. and Phillips, M.: Classical Electricity and Magnetism. Addison-Wesley, Mass., 1956, 400 p.

mean quantity and a fluctuating quantity, one has

$$\frac{\partial \rho_t}{\partial t} + \nabla \cdot \left[ (\bar{\rho} + \rho_t) \quad (\underline{\bar{U}} + \underline{u}) \right] + \frac{1}{\tau} (\bar{\rho} + \rho_t) = 0 \ .$$

Taking the time averages of the above equation and then subtracting these time averaged quantities from the above equation, one gets

$$\frac{\partial \rho_t}{\partial t} + \nabla \cdot \left[ \bar{\rho}\underline{u} + \rho_t \ (\underline{\bar{U}} + \underline{u}) \ -\overline{\rho_t \underline{u}} \right] + \frac{1}{\tau} \rho_t = 0 \ . \qquad (2)$$

Equation 2 is the equation of continuity, in electrodynamics, for the fluctuating and time mean components of $\rho_t$ and $\underline{U}$ in a moving medium.

By introducing the vector and scalar potentials and the Lorentz condition into Maxwell's electrodynamic field equations, it is possible to derive a set of inhomogeneous wave equations. As before, by separating the instantaneous quantities into mean and fluctuating quantities, and by subtracting from the instantaneous wave equation its time averages, one obtains the fundamental differential equation for the potential fluctuations about its mean value as follows [3] :

$$\nabla^2 \psi - \mu\epsilon \frac{\partial^2 \psi}{\partial t^2} - \mu \sigma \frac{\partial \psi}{\partial t} = - \frac{\rho_t}{\epsilon} \ . \qquad (3)$$

Equation 3 requires some further explanation. If the fluid is a good conductor, the second term on the left side will drop out; whereas if the fluid is a good dielectric, the third term on the left side will drop out. Equation 3 in conjunction with equation 2 and the assumption that $\tau \, \bar{U}_{max} n_{max} \ll 1$ gives the following simple relation:

$$\nabla^2 \psi = \frac{1}{\sigma} \ \nabla \cdot \ (\bar{\rho} \ \underline{u}) \qquad (4)$$

Since it is implicit in the foregoing analysis that the fluid is homogeneous in the pipe so that the bulk conductivity of the fluid is constant, the above equation can be rewritten as follows:

$$\nabla \cdot (\sigma \nabla \psi - \bar{\rho}\, \underline{u}) = 0,$$

or

$$\nabla \cdot (\sigma\, \underline{e} - \underline{j}) = 0,$$

where $\underline{e}$ is the fluctuating field intensity or the induced AC field intensity in the sense that it is fluctuating about the induced DC field intensity, and $\underline{j}$ is the fluctuating current density. The fluctuating current density $\underline{j}$ is generated through the transport of the mean true-charge density by the turbulent velocity-fluctuation components. The first term in the parantheasis according to Ohm's law, is also a fluctuating current density due to the induced AC field intensity. Thus the above equation shows a conservation of fluctuating current density in the elemental control volume of fluid.

Let the difference of the fluctuating current densities in each direction be $\Delta j_x$, $\Delta j_r$, and $\Delta j_\theta$, respectively. Equation 4 can then yield as follows:

$$\sigma \frac{\partial \psi}{\partial x} - \bar{\rho} u = \Delta j_x,$$

and

$$\sigma \frac{\partial \psi}{\partial r} - \bar{\rho} v = \Delta j_r, \qquad (5)$$

$$\frac{\sigma}{r} \frac{\partial \psi}{\partial \theta} - \bar{\rho} w - \Delta j_\theta.$$

It is assumed that $\Delta j_x$, $\Delta j_r$, and $\Delta j_\theta$ are always much smaller than the fluctuating current densities due to the velocity fluctuating components and the fluctuating current densities in terms of the induced potential fluctuations gradients. In other words, the fluctuating current densities due to the turbulent flow might be almost counterbalanced in each direction by the corresponding induced potential fluctuation gradients.

Equation 5 constitutes the proposed differential equations for electrokinetic-potential fluctuations. They reveal that the main cause of the electrokinetic-potential fluctuations may be the transport of the mean true-charge density by the corresponding velocity-fluctuation component.

By introducing Fourier transforms and substituting a potential-difference fluctuation between two closely spaced electrodes in lieu of the potential-fluctuation component, Chuang [3] has derived the following equations from the set labeled equation 5:

$$\left.\begin{aligned} E_u(n) &= K_1 \left(\frac{\sigma}{\bar{\rho}}\right)^2 E_{\Delta\psi_x}(n). \\ E_v(n) &= K_2 \left(\frac{\sigma}{\bar{\rho}}\right)^2 E_{\Delta\psi_r}(n), \\ E_w(n) &= K_3 \left(\frac{\sigma}{\bar{\rho}}\right)^2 E_{\Delta\psi_\theta}(n), \\ \text{and} \quad E_{uv}(n) &= K_4 \left(\frac{\sigma}{\bar{\rho}}\right)^2 E_{\Delta\psi_{xr}}(n). \end{aligned}\right\} \quad (6)$$

where the wave number, $n$, is in $cm^{-1}$, $E_{u,\ v,\ w,\ uv,}$ in $cm^3$ per $second^2$, $E_{\Delta\psi}$ in $volt^2$ - cm, $\bar{\rho}$ in coul per $m^3$ and $\sigma$ in mhos per m. All K's are arbitrary constants. Equation 6 shows that, for a given fluid at a constant temperature, the spectral distributions of turbulent energies and shearing stress are directly proportional to the corresponding energy spectral distributions of the electrokinetic-potential fluctuation difference.

An electrical double layer is presumed to exist at the solid-liquid interface between the probe which contains the closely spaced electrodes and the water. However, the thickness of the diffused double layer seems irrelevant in the preceding analysis.

## CONCLUSIONS

1. The electrokinetic-potential fluctuations at any point in the flow field of fully developed pipe flow of distilled water are measurable.

2. The assumed relation between the electrokinetic-potential fluctuations and the turbulent velocity fluctuations given by equations 5 and 6 are supported by the experiment.

3. The inferred turbulent intensities and shearing stress are in good agreement with Laufer and Sandborn's hot-wire anemometer data for air flow through a pipe at the same mean Reynolds number.

4. The inferred energy spectra indicate some characteristics of the turbulent shear flow at low Reynolds number and are in good agreement with Sandborn's anemometer data for $Re = 5 \times 10^4$ in air flow.

5. The technique of electrokinetic-potential fluctuation measurements may be valuable for research on turbulence in fluids.

## ACKNOWLEDGEMENTS

Valuable discussion with Dr. L. V. Baldwin is sincerely appreciated. Financial support provided by the National Science Foundation for this study is gratefully acknowledged.

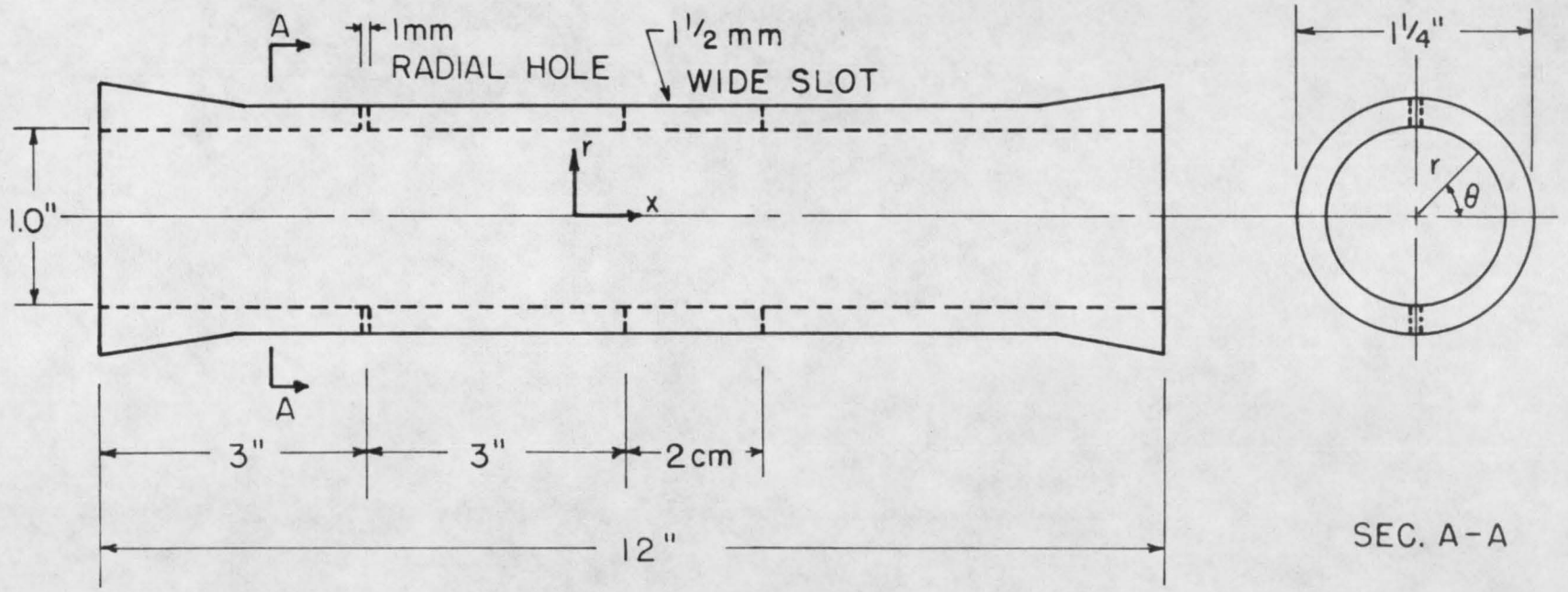
A
1mm
RADIAL HOLE
1½ mm
WIDE SLOT
r
x
1.0"
A
3"
3"
2cm
12"
1¼"
r
θ
SEC. A-A

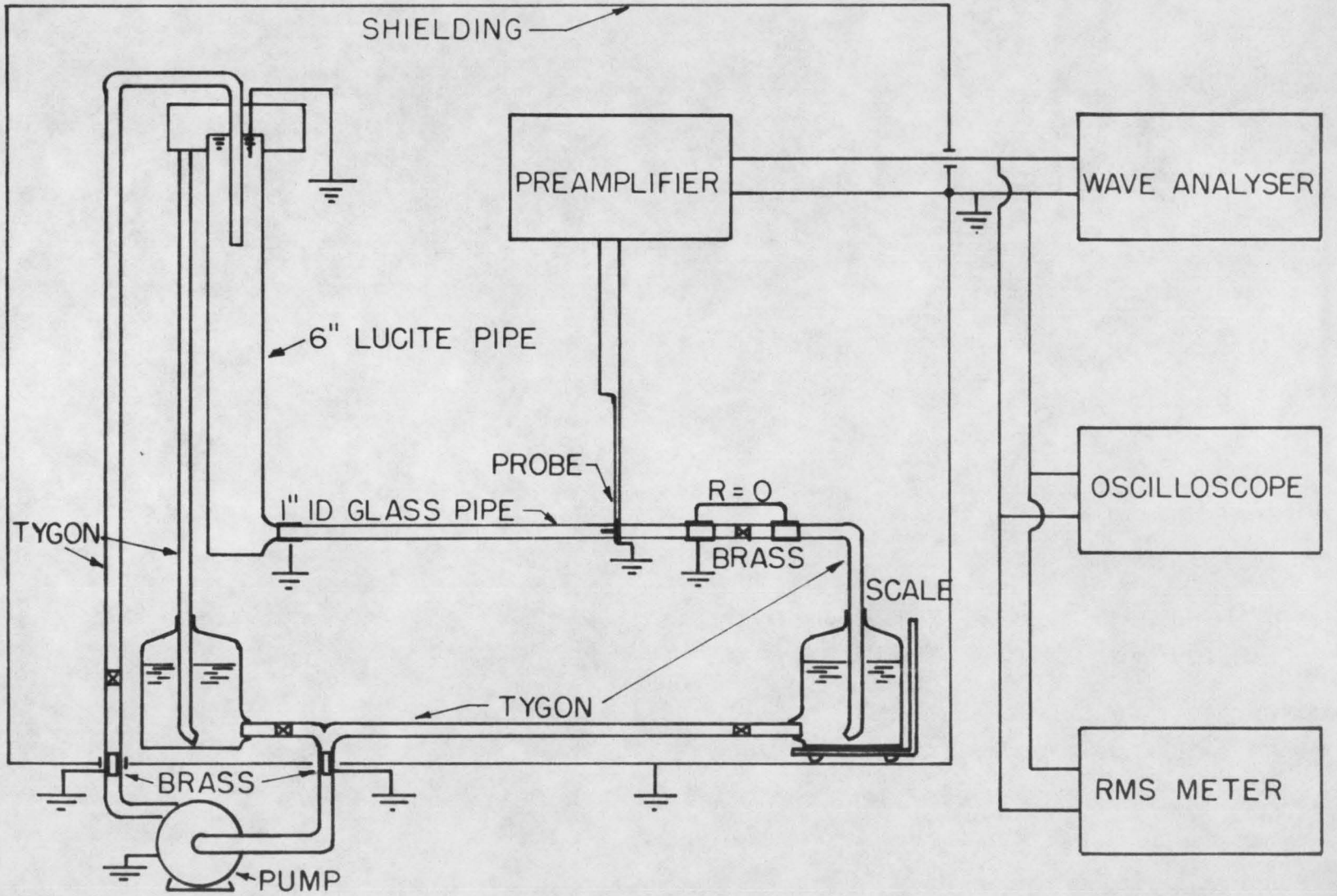
SHIELDING
PREAMPLIFIER
WAVE ANALYSER
6" LUCITE PIPE
PROBE
R = 0
1" ID GLASS PIPE
TYGON
BRASS
OSCILLOSCOPE
SCALE
TYGON
BRASS
RMS METER
PUMP

Fig. 2

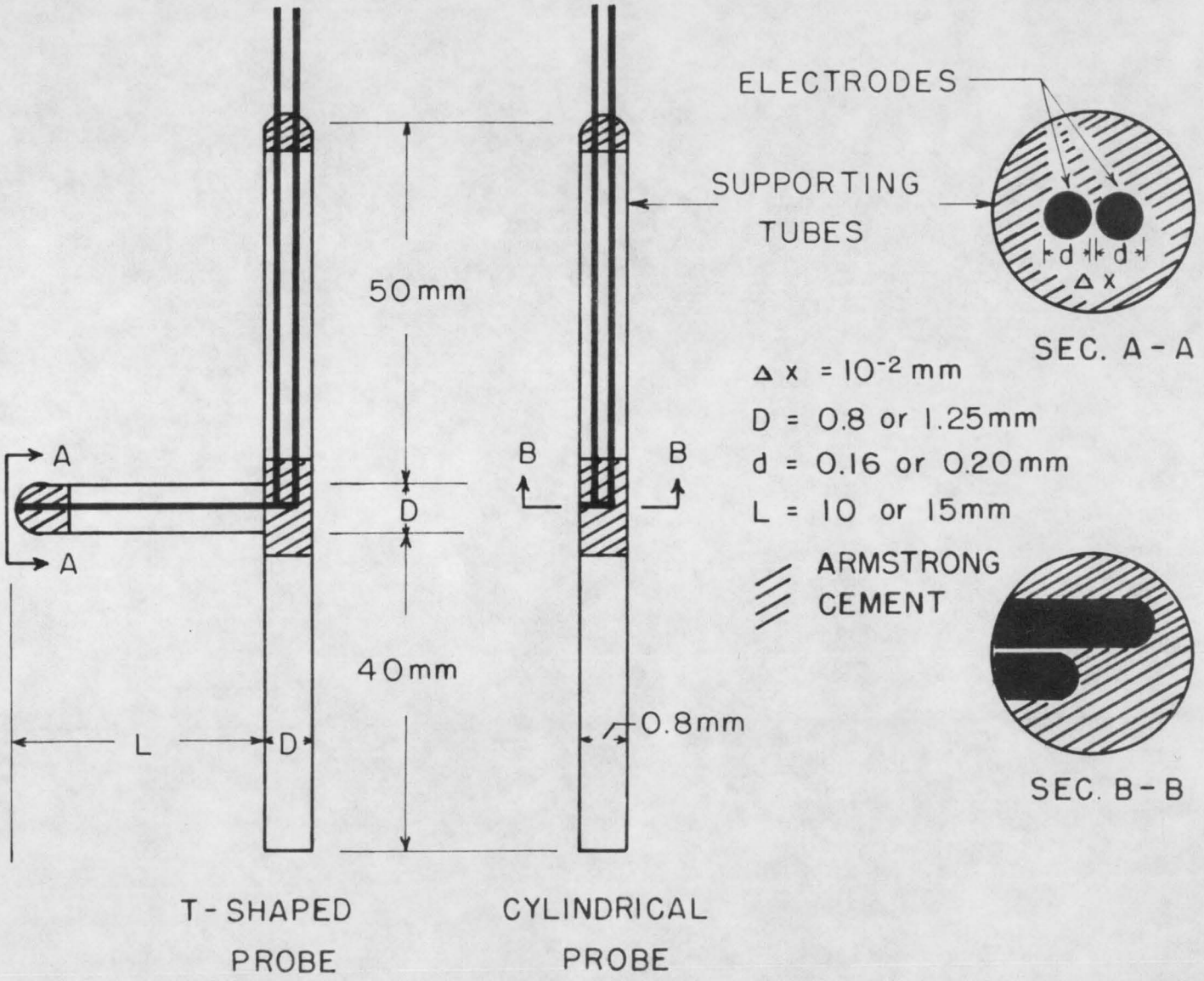
ELECTRODES
SUPPORTING TUBES
d
d
Δ x
SEC. A - A
Δ x = 10⁻² mm
D = 0.8 or 1.25mm
d = 0.16 or 0.20 mm
L = 10 or 15mm
ARMSTRONG CEMENT
SEC. B - B
A
A
B
B
50mm
D
40mm
L
D
0.8mm
T - SHAPED PROBE
CYLINDRICAL PROBE

Fig. 3

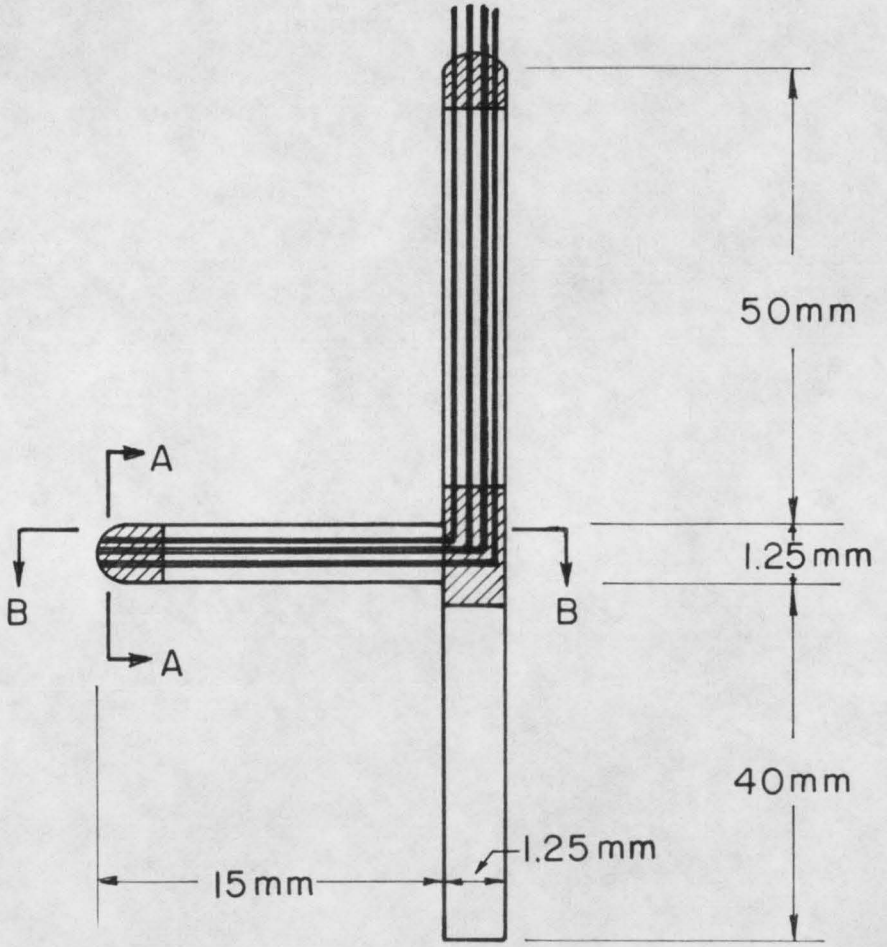


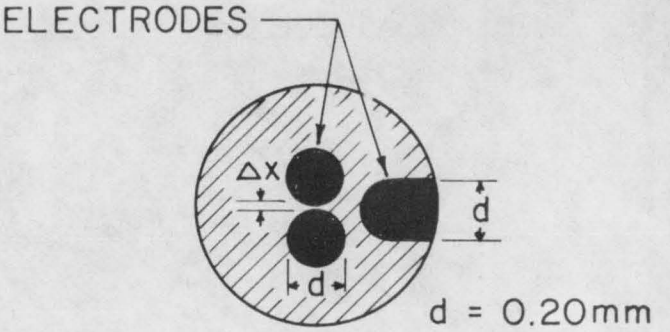


SEC. A-A

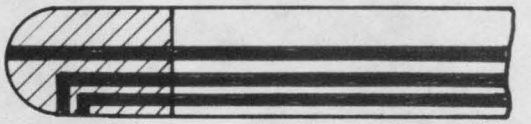

SEC. B-B

Fig. 4

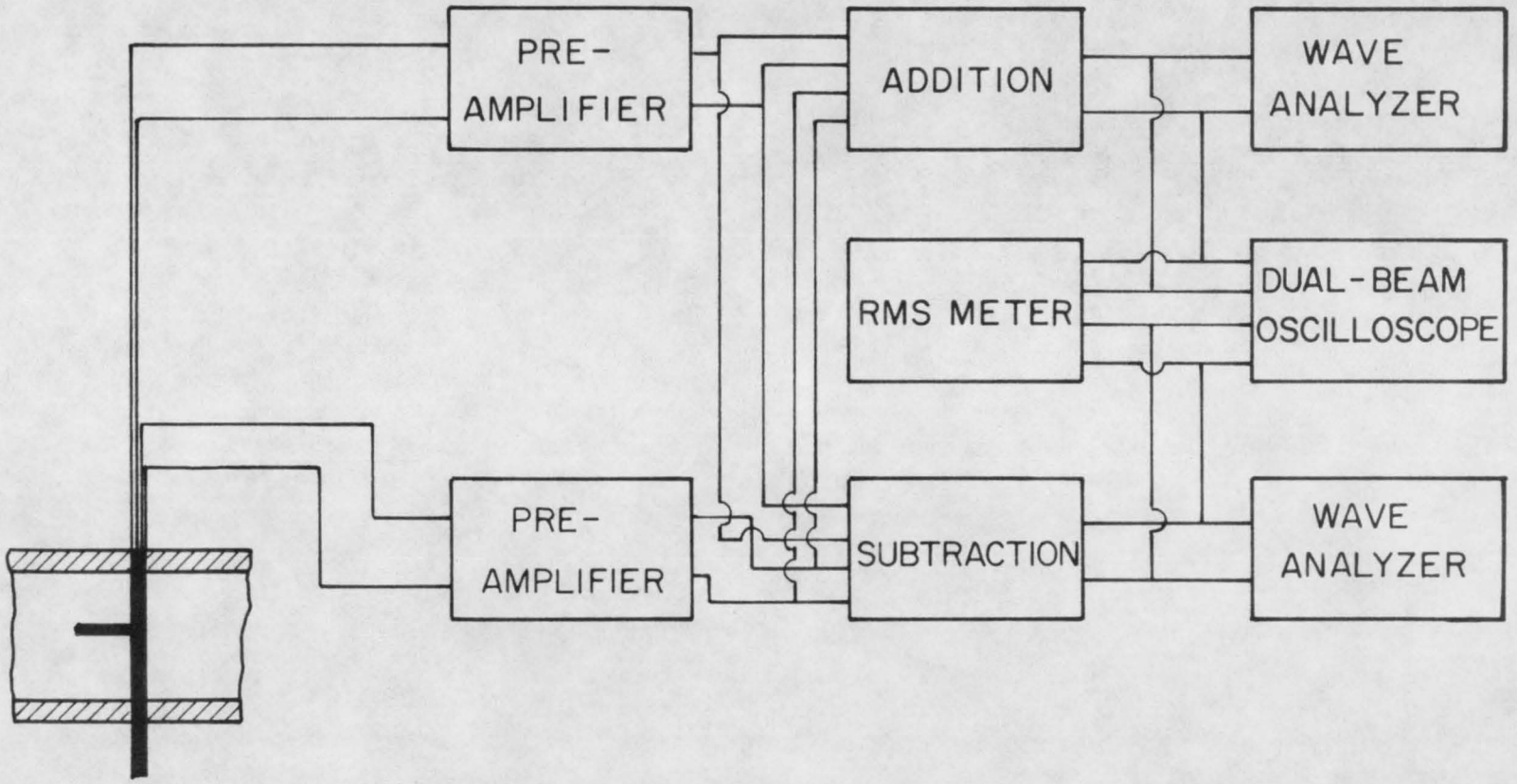
PRE-
AMPLIFIER
ADDITION
WAVE
ANALYZER
RMS METER
DUAL-BEAM
OSCILLOSCOPE
PRE-
AMPLIFIER
SUBTRACTION
WAVE
ANALYZER

Fig. 5

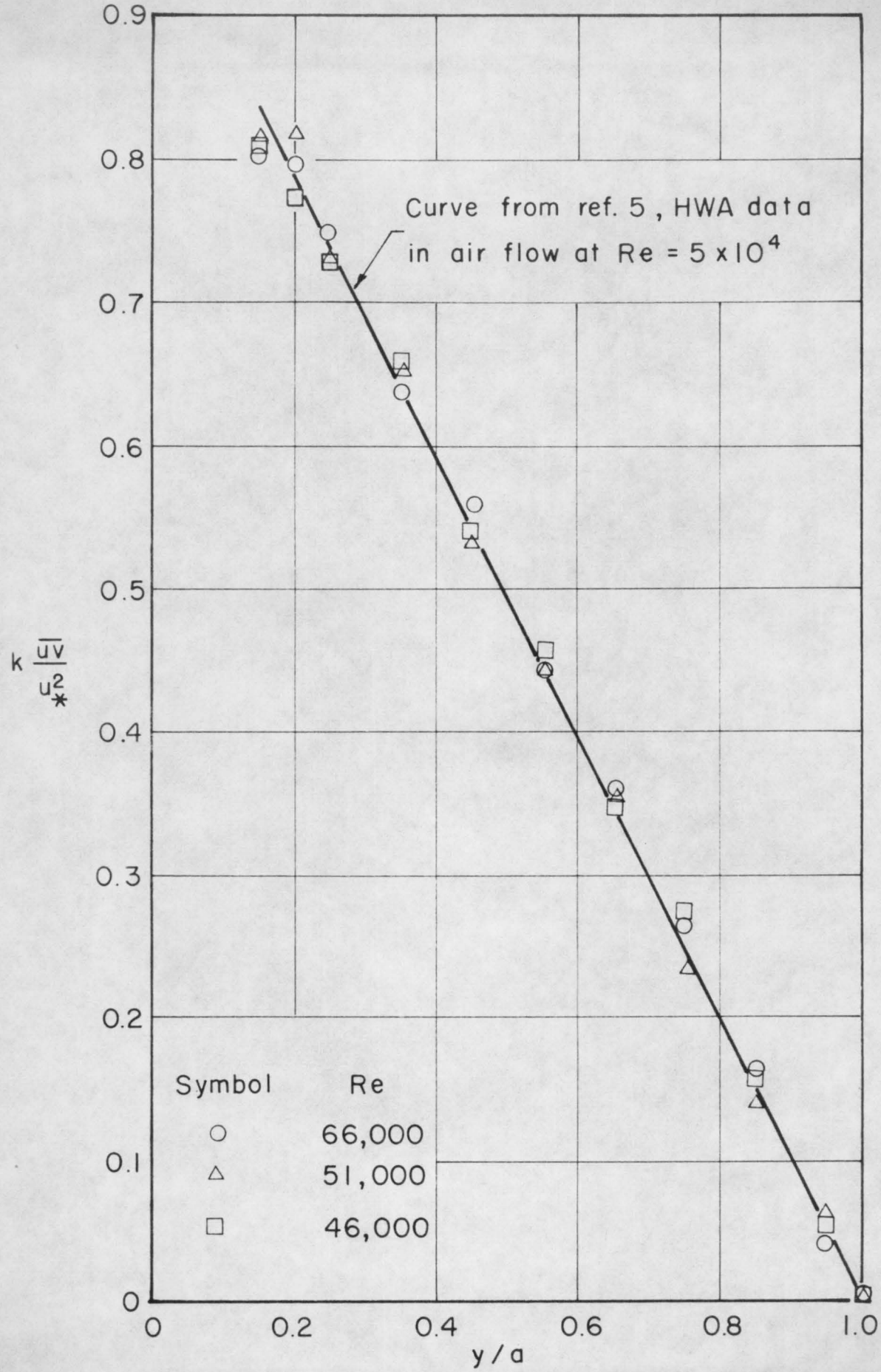
0.9
0.8
0.7
0.6
0.5
0.4
0.3
0.2
0.1
0
0
0.2
0.4
0.6
0.8
1.0
y/a
$k \frac{\overline{uv}}{u_*^2}$
Curve from ref. 5, HWA data
in air flow at Re = 5 x 10⁴
Symbol
Re
66,000
51,000
46,000

Fig 6.

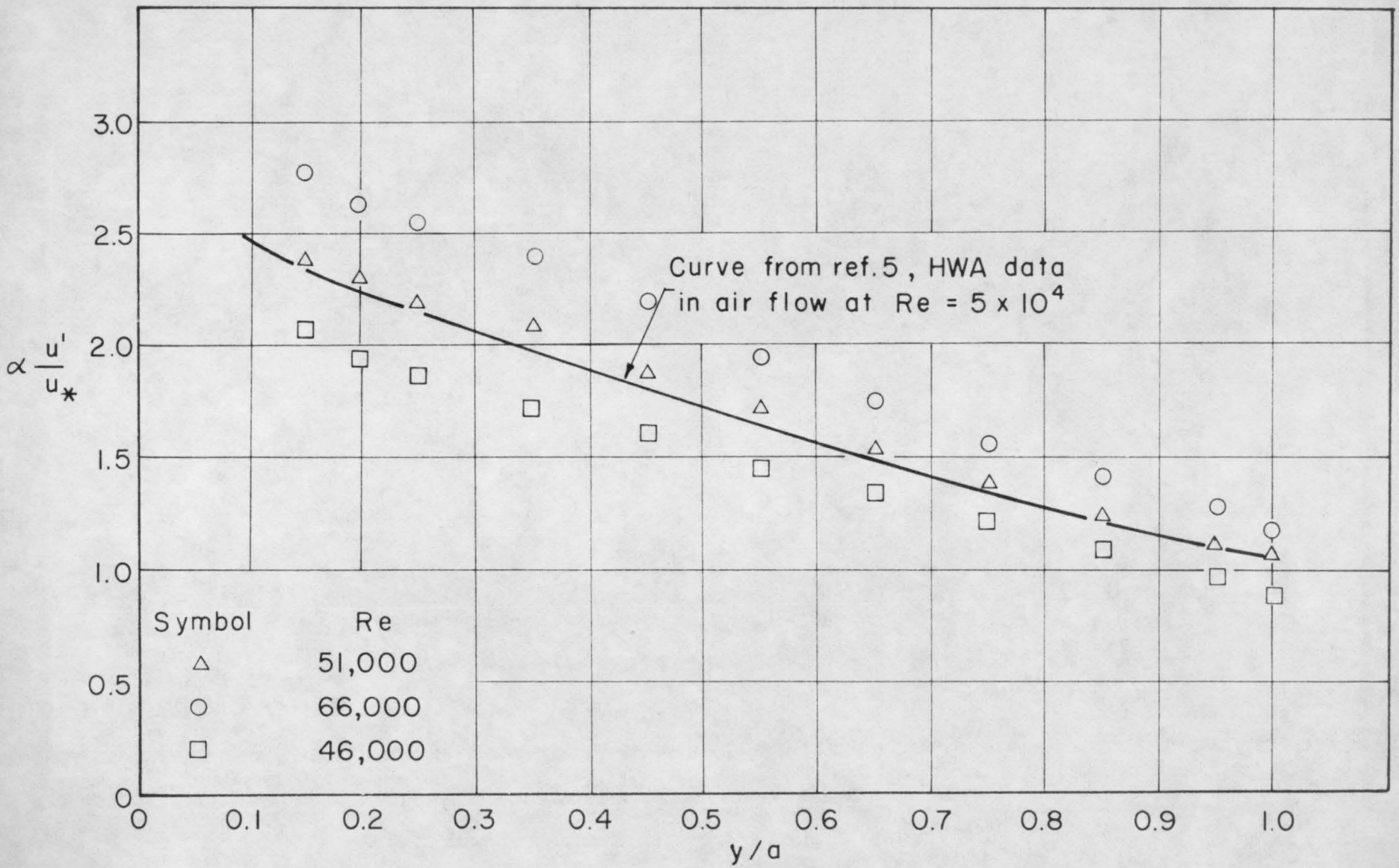
Curve from ref.5, HWA data
in air flow at Re = 5 x 10^4
Symbol
Re
51,000
66,000
46,000
α u'/u*
y/a
0
0.5
1.0
1.5
2.0
2.5
3.0
0.1
0.2
0.3
0.4
0.5
0.6
0.7
0.8
0.9
1.0

Fig. 7.

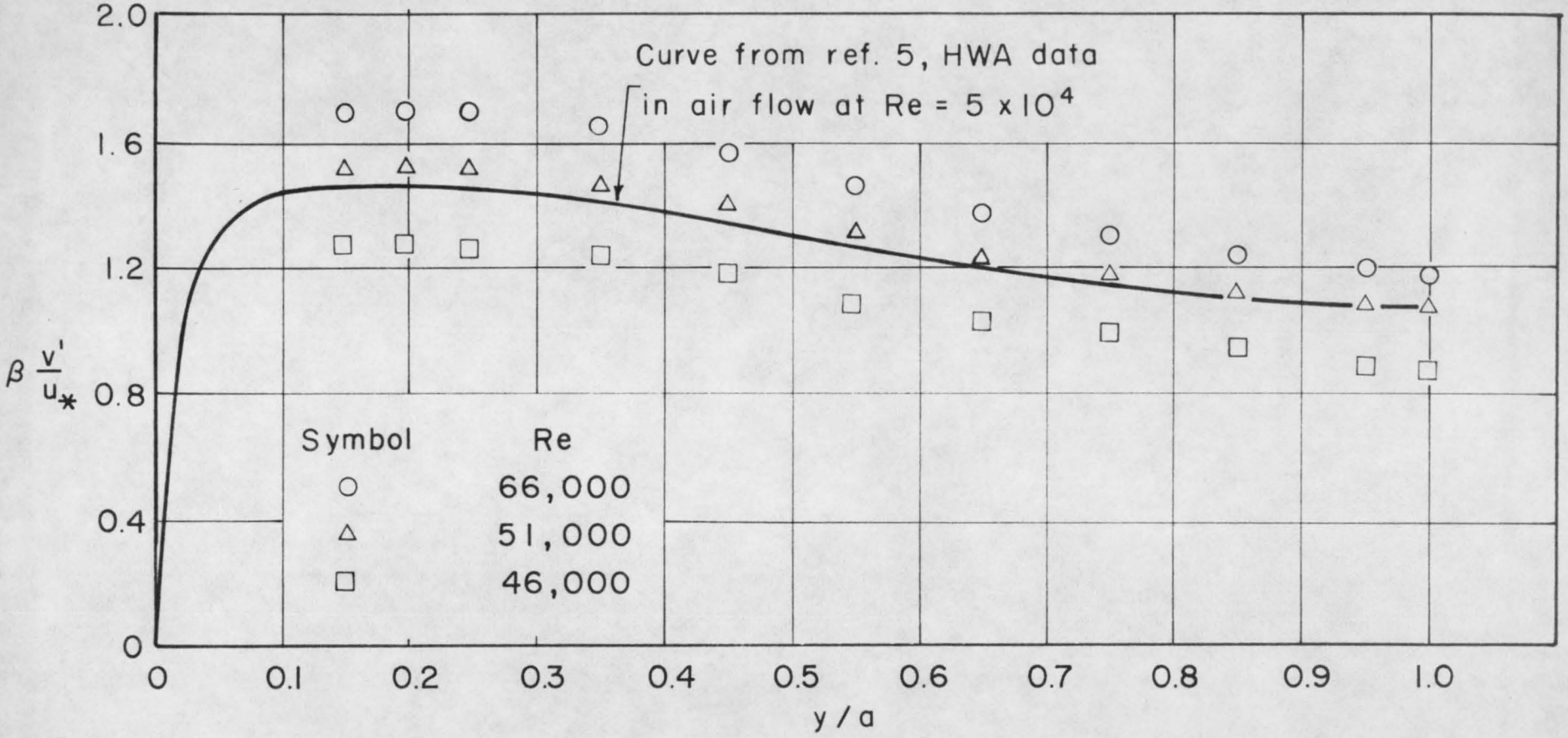
Curve from ref. 5, HWA data
in air flow at Re = 5 x 10^4
Symbol
Re
66,000
51,000
46,000
β v'/u*
y/a
2.0
1.6
1.2
0.8
0.4
0
0
0.1
0.2
0.3
0.4
0.5
0.6
0.7
0.8
0.9
1.0

Fig. 8

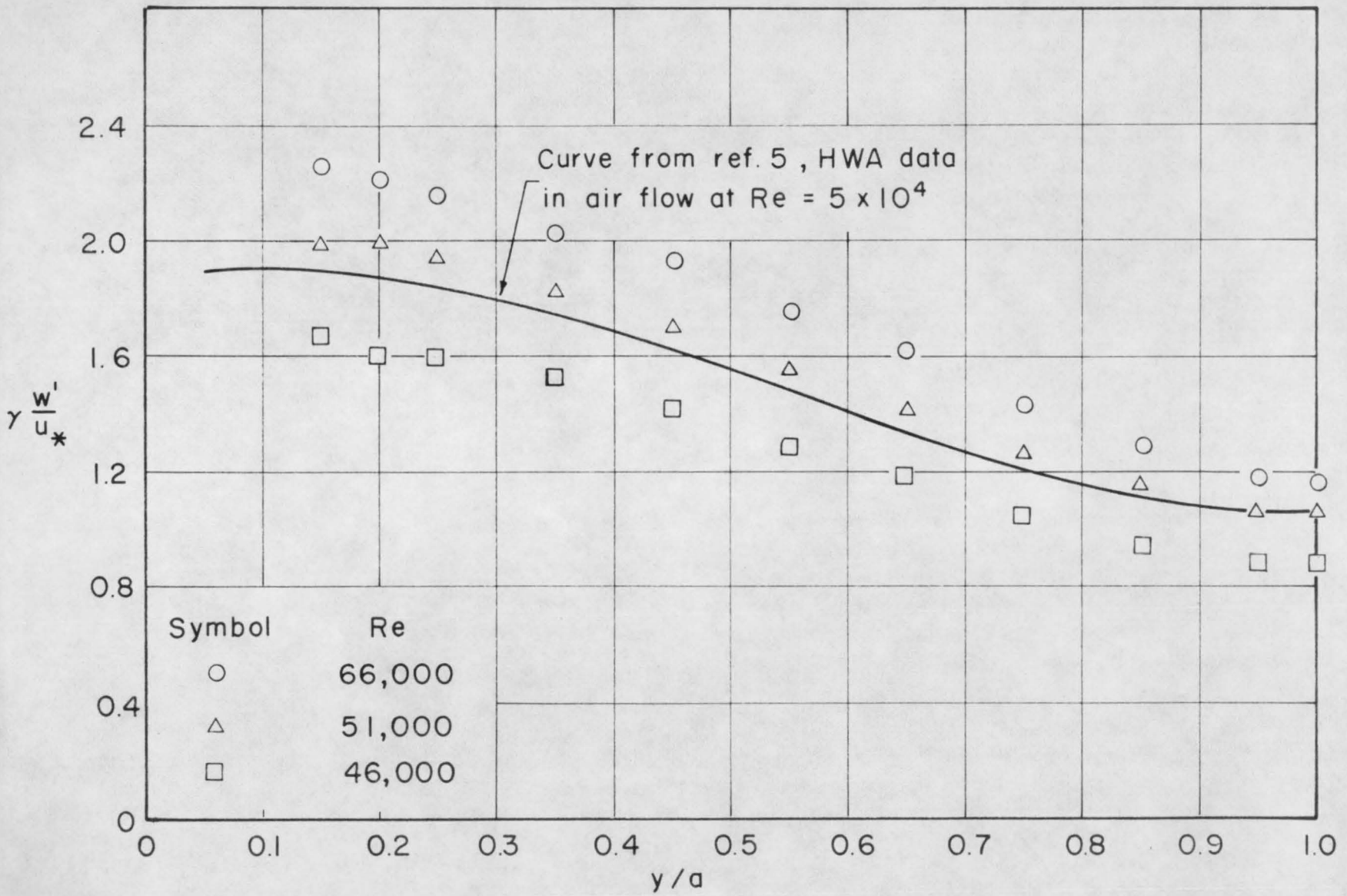
Curve from ref. 5 , HWA data
in air flow at Re = 5 x 10⁴
Symbol
Re
66,000
51,000
46,000
2.4
2.0
1.6
1.2
0.8
0.4
0
0
0.1
0.2
0.3
0.4
0.5
0.6
0.7
0.8
0.9
1.0
y/a
γ w'/u*

Fig. 9

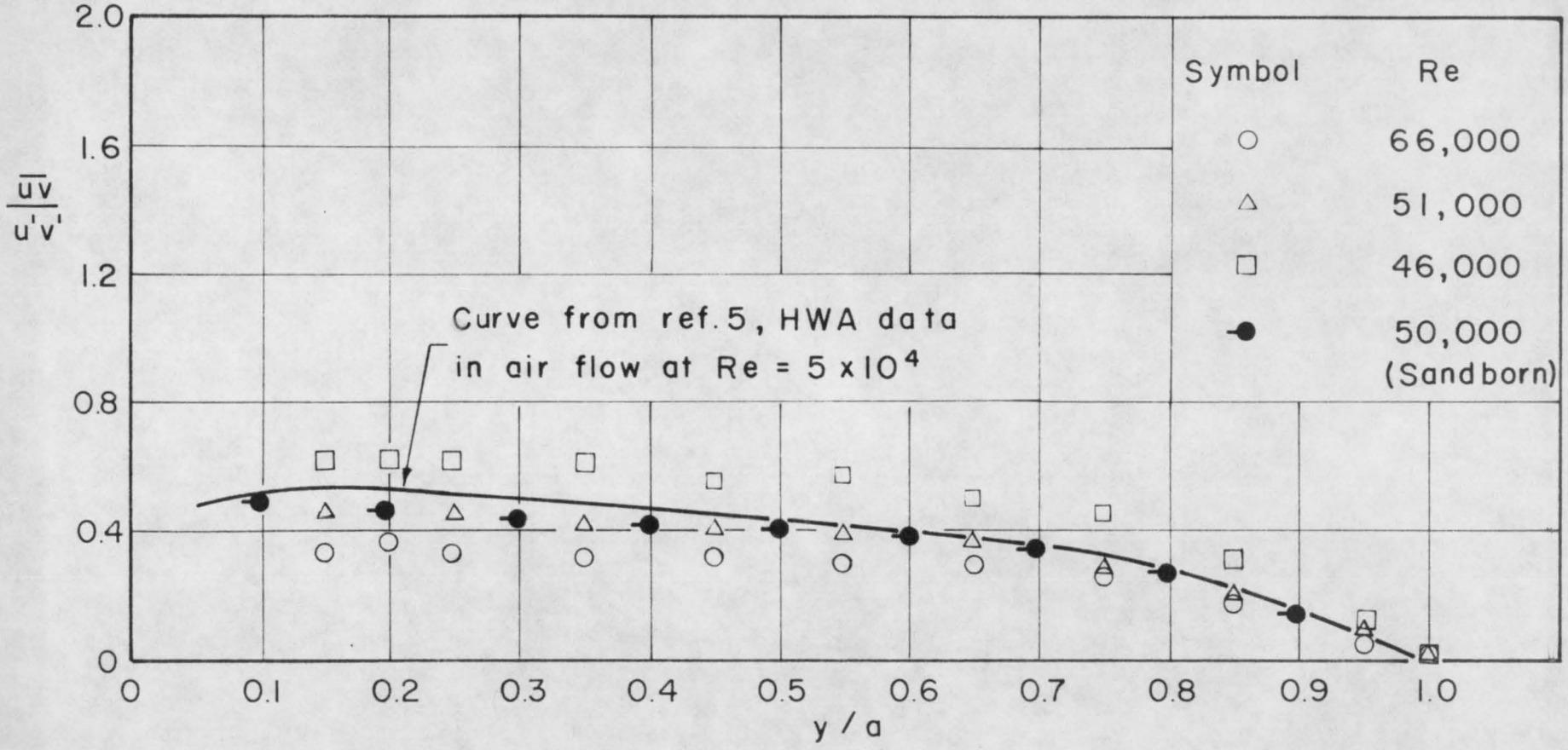


H. Chuang Fig. 10.

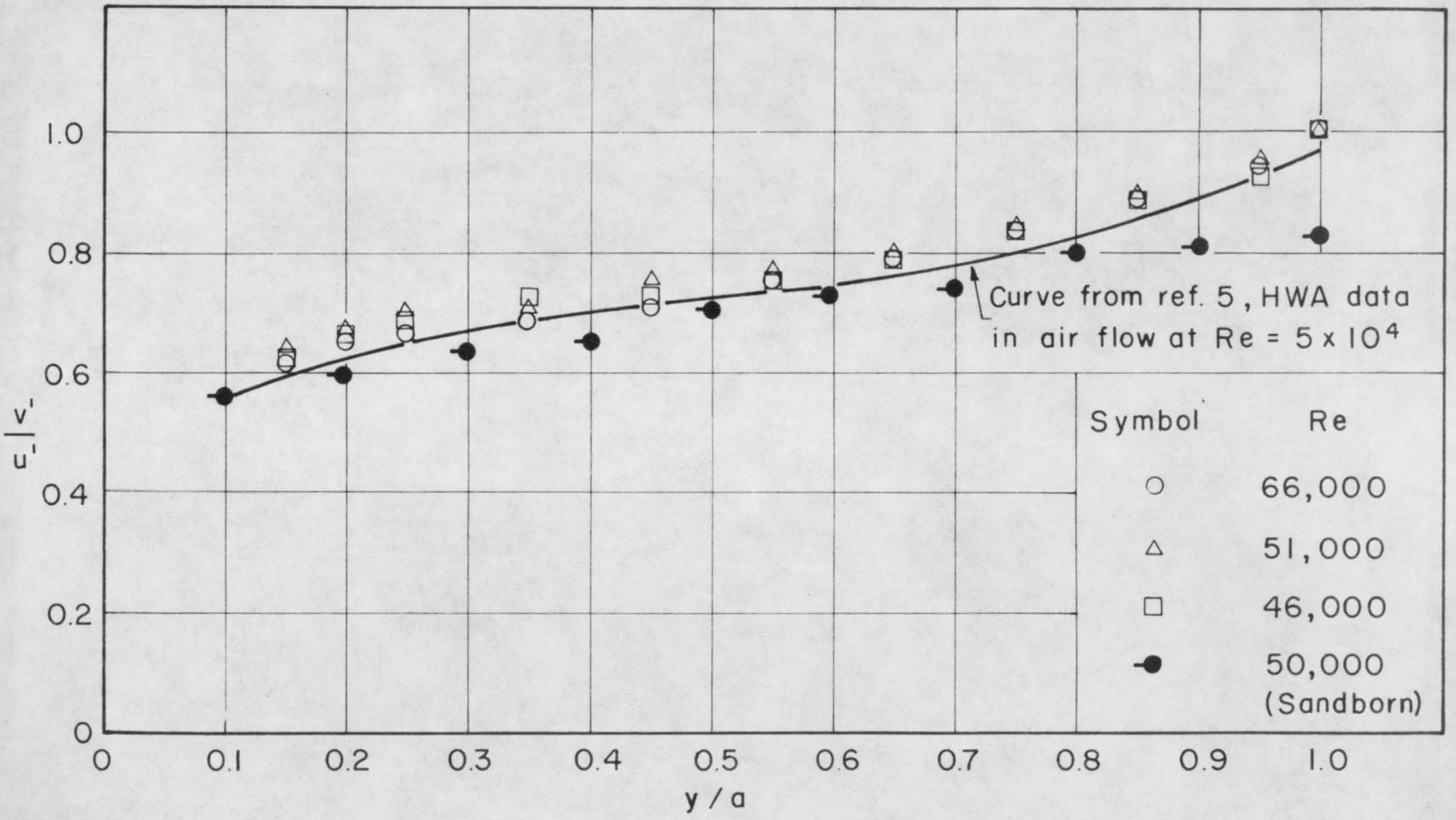
1.0
0.8
0.6
0.4
0.2
0
u'/v'
0
0.1
0.2
0.3
0.4
0.5
0.6
0.7
0.8
0.9
1.0
y / a
Curve from ref. 5, HWA data in air flow at Re = 5 x 10⁴
Symbol
Re
66,000
51,000
46,000
50,000 (Sandborn)

Fig. 11

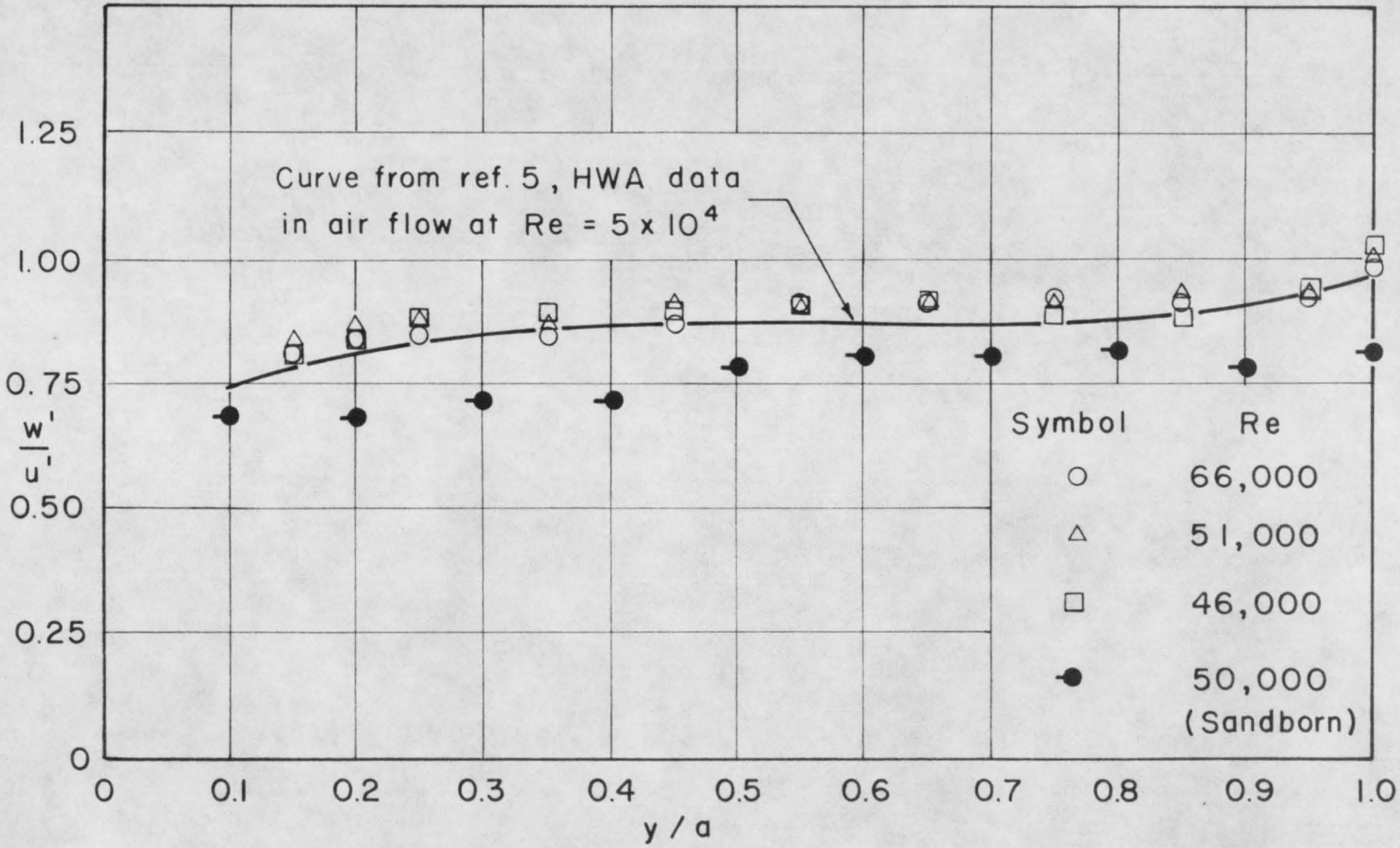
Curve from ref. 5, HWA data
in air flow at Re = 5 x 10^4
Symbol
Re
66,000
51,000
46,000
50,000
(Sandborn)
1.25
1.00
0.75
0.50
0.25
0
w'/u'
0
0.1
0.2
0.3
0.4
0.5
0.6
0.7
0.8
0.9
1.0
y / a

Fig. 12.

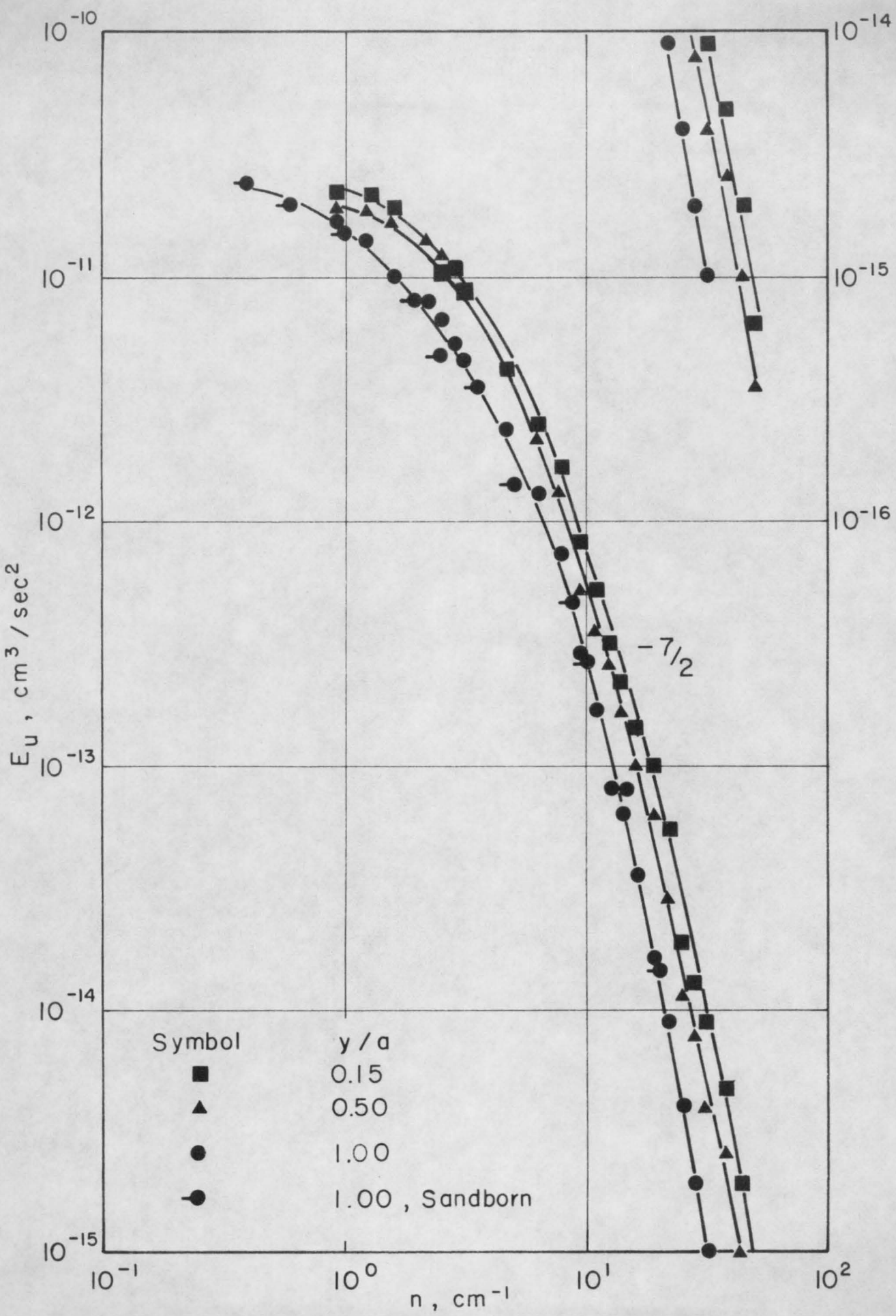
$10^{-10}$
$10^{-11}$
$10^{-12}$
$10^{-13}$
$10^{-14}$
$10^{-15}$
$10^{-14}$
$10^{-15}$
$10^{-16}$
$E_u$ , $cm^3$ / $sec^2$
$-7/2$
Symbol
y / a
0.15
0.50
1.00
1.00 , Sandborn
$10^{-1}$
$10^{0}$
$10^{1}$
$10^{2}$
n , $cm^{-1}$

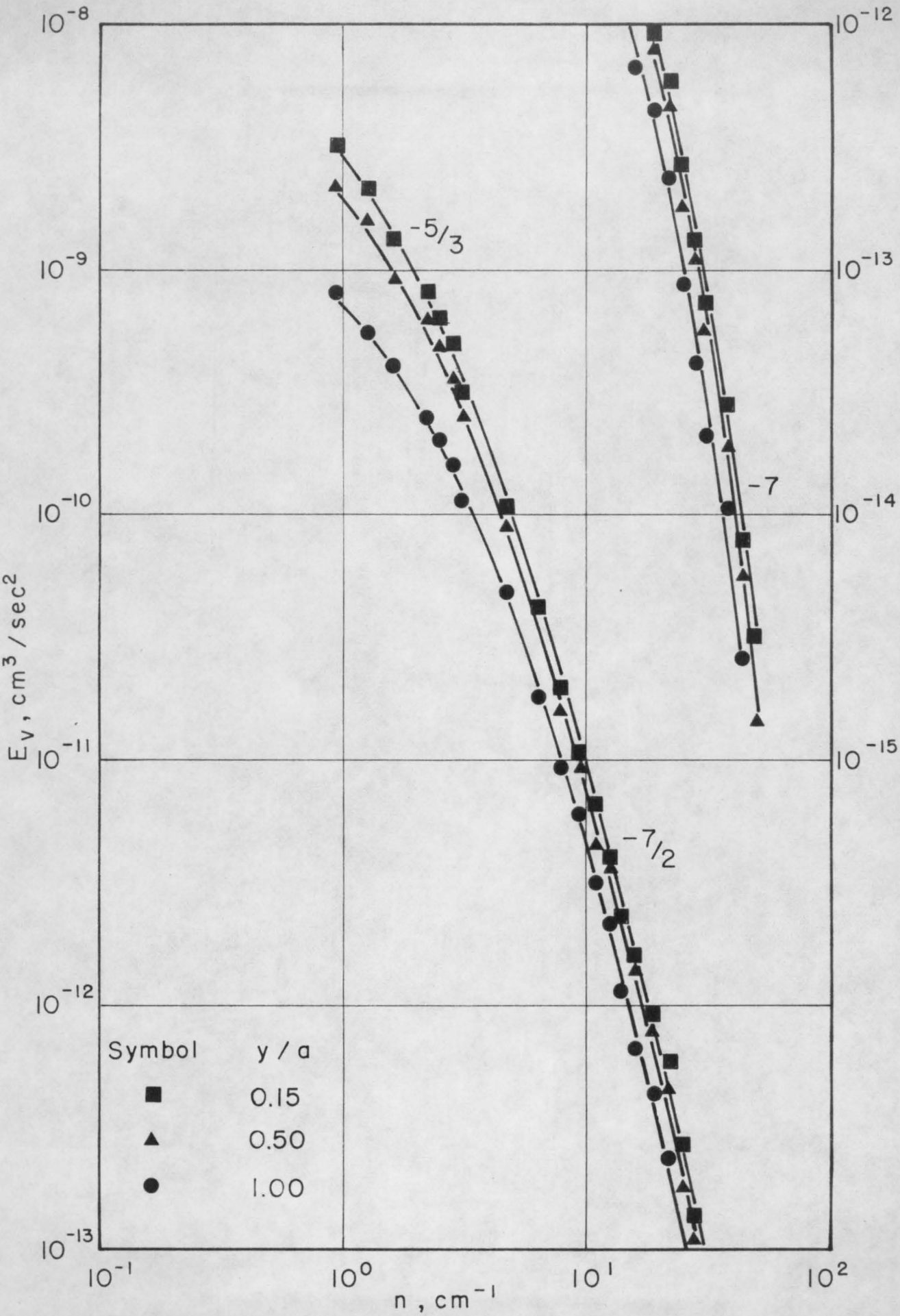
$10^{-8}$
$10^{-9}$
$10^{-10}$
$10^{-11}$
$10^{-12}$
$10^{-13}$
$10^{-12}$
$10^{-13}$
$10^{-14}$
$10^{-15}$
$E_v$, $cm^3/sec^2$
-5/3
-7
-7/2
Symbol
y / a
0.15
0.50
1.00
$10^{-1}$
$10^{0}$
$10^{1}$
$10^{2}$
n , $cm^{-1}$

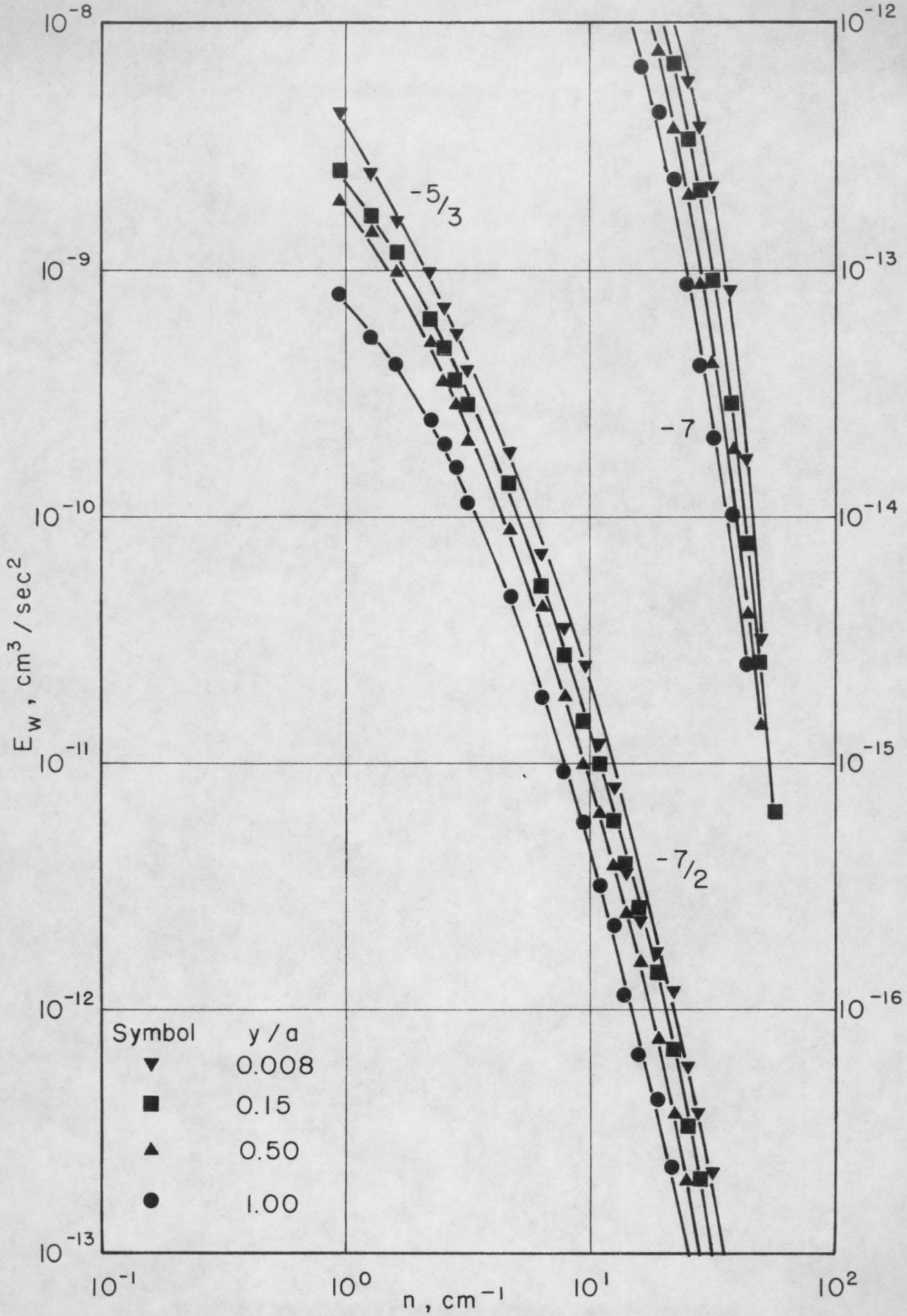
$10^{-8}$
$10^{-9}$
$10^{-10}$
$10^{-11}$
$10^{-12}$
$10^{-13}$
$10^{-12}$
$10^{-13}$
$10^{-14}$
$10^{-15}$
$10^{-16}$
$E_w$ , $cm^3/sec^2$
-5/3
-7
-7/2
Symbol
y / a
0.008
0.15
0.50
1.00
$10^{-1}$
$10^{0}$
$10^{1}$
$10^{2}$
n , $cm^{-1}$

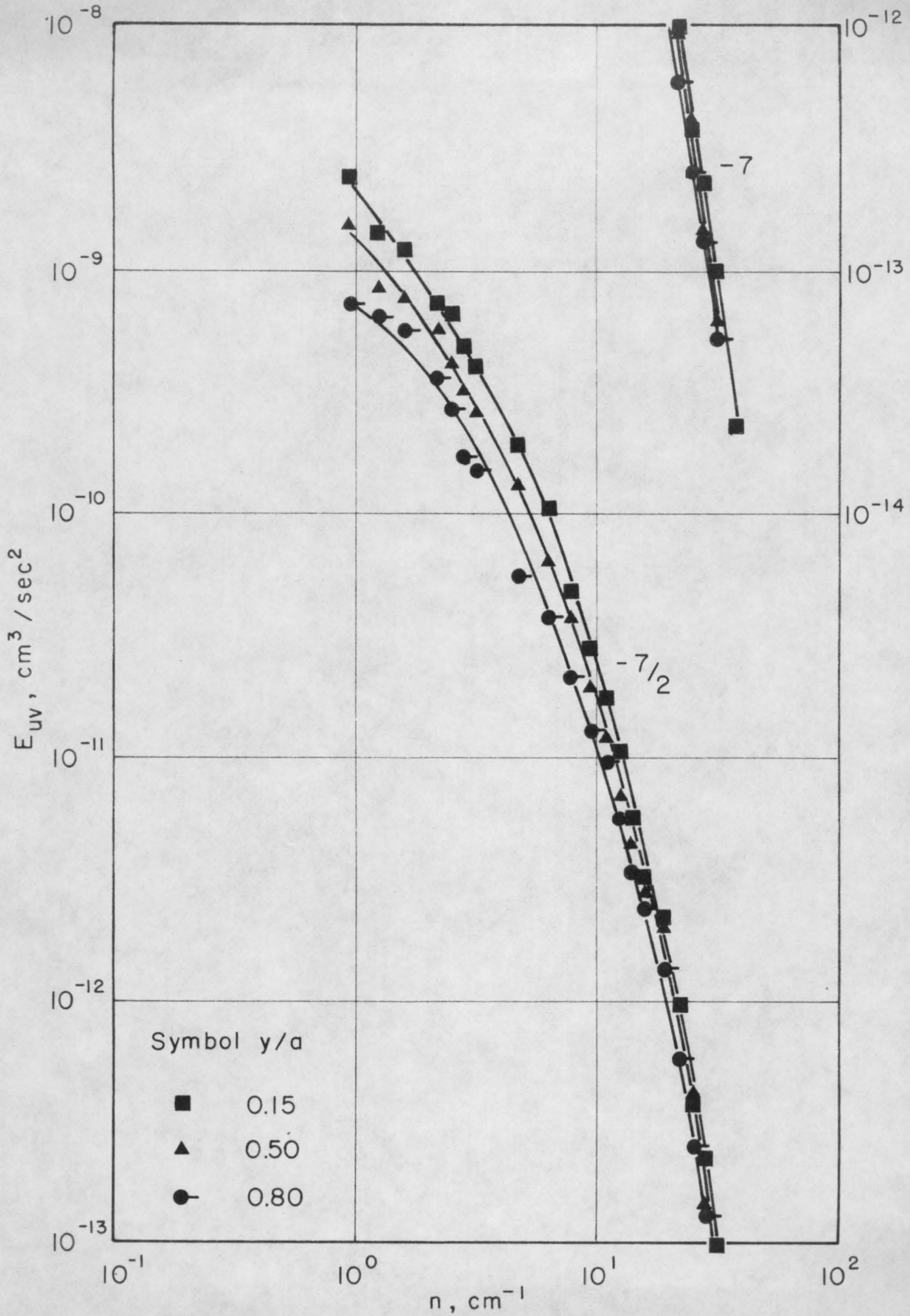
$10^{-8}$
$10^{-9}$
$10^{-10}$
$10^{-11}$
$10^{-12}$
$10^{-13}$
$10^{-12}$
$10^{-13}$
$10^{-14}$
$E_{uv}$, $cm^3/sec^2$
-7
$-7/2$
Symbol y/a
0.15
0.50
0.80
$10^{-1}$
$10^{0}$
$10^{1}$
$10^{2}$
n, $cm^{-1}$